OPEN

Light: Science & Applications (2017) 6, e16258; doi:10.1038/lsa.2016.258
Official journal of the CIOMP 2047-7538/17
www.nature.com/lsa

ORIGINAL ARTICLE

Plasmon-assisted optical trapping and anti-trapping

Aliaksandra Ivinskaya[1], Mihail I Petrov[1], Andrey A Bogdanov[1], Ivan Shishkin[2], Pavel Ginzburg[1,2] and Alexander S Shalin[1,3,4]

The ability to manipulate small objects with focused laser beams has opened a venue for investigating dynamical phenomena relevant to both fundamental and applied science. Nanophotonic and plasmonic structures enable superior performance in optical trapping via highly confined near-fields. In this case, the interplay between the excitation field, re-scattered fields and the eigenmodes of a structure can lead to remarkable effects; one such effect, as reported here, is particle trapping by laser light in a vicinity of metal surface. Surface plasmon excitation at the metal substrate plays a key role in tailoring the optical forces acting on a nearby particle. Depending on whether the illuminating Gaussian beam is focused above or below the metal-dielectric interface, an order-of-magnitude enhancement or reduction of the trap stiffness is achieved compared with that of standard glass substrates. Furthermore, a novel plasmon-assisted anti-trapping effect (particle repulsion from the beam axis) is predicted and studied. A highly accurate particle sorting scheme based on the new anti-trapping effect is analyzed. The ability to distinguish and configure various electromagnetic channels through the developed analytical theory provides guidelines for designing auxiliary nanostructures and achieving ultimate control over mechanical motion at the micro- and nano-scales.

Light: Science & Applications (2017) **6,** e16258; doi:10.1038/lsa.2016.258; published online 5 May 2017

Keywords: Gaussian beam; Green's function; optical forces; optical tweezers; surface plasmon

INTRODUCTION

Trapping and manipulation by micro- and nano-scale objects contributes to the development of various aspects of multidisciplinary science by pushing the limits of widely employed classical characterization tools and fabrication techniques[1]. Traditionally, optical trapping of micron-sized objects is achieved by using tightly focused Gaussian beams, e.g., fundamental modes of a laser[2]. Carefully designed interference patterns created with dynamically reconfigurable holograms enable simultaneous trapping of several particles and even the creation of three-dimensional artificial crystals[3,4]. The stiffness of optical traps and subsequent particle localization can be controlled by employing hollow beams, higher-order Gauss–Hermite and Gauss–Laguerre modes, etc[5–7]. Trapping schemes employing structured light beams play a major role in many experiments. For example, excitation can be either a single mode or a combination of several modes and either propagating or evanescent. Nonlinear (quadratic) dependence of optical forces on the field amplitude brings unique features inherent to a particular illumination scheme since contributions of individual modes are not additive[8]. This free-space optical approach, however, faces some limitations resulting from the classical diffraction limit, and achieving nanoscale localization requires introduction of auxiliary structures featuring highly confined near fields[9–17]. Metals have negative permittivity at visible and infrared spectral ranges and can support localized electromagnetic excitations (plasmon resonances), thereby surpassing the classical diffraction limit[9–11]. Plasmonic tweezers utilize highly confined electromagnetic fields for the trapping of nanoscale particles in the vicinity of nano-antennas[12–14]. Localization down to tens of nanometers was shown in Refs. 13,15, and ordered positioning of nanoparticles in arrays was demonstrated in Refs. 16,17.

While plasmonic nano-antennas (typical layout of plasmonic tweezers) provide a set of well-defined localized optical traps, this approach is not always suitable for applications where dynamical control over particle position is required. Alternatively, potential abilities of flat unstructured substrates used for improving trapping characteristics, first demonstrated a decade ago[18] and more recently with 'surface plasmon virtual probe' excited by focused light[19], are still overlooked. Recently, planar geometries were shown to enable several novel effects in the field of optical forces. The emergence of substrate-assisted lateral forces was proposed in several configurations, e.g., chiral particles with circularly polarized light excitation[20] and dielectric beads under inclined plane wave illumination[21]. Optical attraction (tractor beams) via an excitation of surface plasmon at the substrate at grazing angle illumination was demonstrated[22] without requiring sophisticated substrates[23].

While optical forces in the 'particle next to a surface' geometries were widely studied[20–22], in all those cases, a plane wave illumination was considered. However, in most experiments, tightly focused beams containing many spatial harmonics are employed. Those spatial

[1]Department of Nanophotonics and Metamaterials, ITMO University, Birzhevaja Line, 14, 199034 St Petersburg, Russia; [2]School of Electrical Engineering, Tel Aviv University, Ramat Aviv, Tel Aviv 69978, Israel; [3]Kotel'nikov Institute of Radio Engineering and Electronics of Russian Academy of Sciences (Ulyanovsk branch), Goncharova Street 48/2, 432071 Ulyanovsk, Russia and [4]Ulyanovsk State University, Lev Tolstoy Street 42, 432017 Ulyanovsk, Russia
Correspondence: AS Shalin, Email: alexandesh@gmail.com
Received 12 July 2016; revised 26 October 2016; accepted 23 November 2016; accepted article preview online 28 November 2016

harmonics interact with auxiliary structures, creating nontrivial interference patterns. Here, the performance of optical tweezers formed by normally incident Gaussian beams on a metal substrate is studied. Varying the focal spot position with respect to the substrate gives an additional degree of freedom in optical manipulation (Figure 1 summarizes the setup). Improved optical trapping and particle repulsion (anti-trapping) are demonstrated for the first time by performing a comprehensive analysis of a self-consistent electromagnetic problem, which focuses on a clear plasmonic signature of the effect.

MATERIALS AND METHODS

Force calculation using a self-consistent field

Optical force acting on a subwavelength particle can be estimated by replacing the particle with a point dipole of polarizability α, which depends on the geometry and material composition of the object. The components of the time-averaged force in the dipole approximation are[24]:

$$F_j = \frac{1}{2}\Re(\alpha \mathbf{E}\partial_j \mathbf{E}^*) \tag{1}$$

where $\mathbf{E}$ is a local field at the place of the particle. The total local field should be calculated self-consistently, taking into account mutual interactions between the particle and the surrounding media. First, the background field ($\tilde{\mathbf{E}}^0$) is calculated, including the incident waves together with the reflections from the structured environment in which the particle is going to be placed. To account for a re-scattered field from the particle itself, Green's function $\hat{\mathbf{G}}$ representing response of the structure to a point dipole source should be derived. Spectral decomposition of the Green's function (Supplementary Information A) enables identification of the propagating and evanescent modes. Exclusion of the latter terms from the series provides a tool for estimating their contributions to the total optical force. Note that straightforward numerical calculations are lacking this ability.

For the excitation by a beam of frequency ω with its magnetic field directed along the y axis (p polarization, see Figure 1), the force components (Supplementary Information B and C) are given by

$$\begin{aligned} F_x &= \tfrac{1}{2}\Re(\alpha \mathbf{E}\partial_x \tilde{\mathbf{E}}^{0*}) + |\alpha|^2\omega^2\mu_1\mu_0 \mathrm{Im}(\mathrm{E}_x E_z^*)\mathrm{Im}(\partial_x G_{xz}) \\ F_z &= \tfrac{1}{2}\Re(\alpha \mathbf{E}\partial_z \tilde{\mathbf{E}}^{0*}) + \\ &\tfrac{1}{2}|\alpha|^2\omega^2\mu_1\mu_0(|\mathrm{E}_x|^2\Re(\partial_z G_{xx}) + |\mathrm{E}_z|^2\Re(\partial_z G_{zz})) \end{aligned} \tag{2}$$

where μ_0 and μ_1 are permeability of vacuum and upper half-space. The transverse force at the wavelength of surface plasmon resonance (Supplementary Information D) can be approximated by

$$F_x^{\mathrm{ap}} = |\alpha|^2\omega^2\mu_1\mu_0 \mathrm{Im}(\tilde{\mathrm{E}}_x^0\tilde{\mathrm{E}}_z^{0*})\mathrm{Im}(\partial_x G_{xz}) \tag{3}$$

Self-induced back action comes into play through the scattered field returning to the particle after the reflection from the substrate. This action is governed by Green's function, which has a pole at the plasmon resonance[21]. The derivative of Green's function with respect to the x coordinate (details are at Supplementary Equation S2) is a non-diagonal matrix and, as a result, the product of different electric field components has a significant impact on the horizontal force, with strong dependence on the polarization. Importantly, variation of the excitation field can change the sign of $\mathrm{Im}(\mathrm{E}_x\mathrm{E}_z^*)$ and subsequently F_x sign (see Equation (2) and Supplementary Information D). The Green's function derivative along the z coordinate (Supplementary Equation S3) retains the diagonal form, and the second term in the vertical force F_z depends only on the modulus of individual field components. As a remark, several approaches[19,21] utilize a dipole moment of the particle $\mathbf{p} = \alpha\mathbf{E} = \hat{\alpha}^{\mathrm{eff}}\tilde{\mathbf{E}}^0$, where the effective polarizability $\hat{\alpha}^{\mathrm{eff}}$ is a diagonal tensor for the coupled particle–substrate system (Supplementary Equation S11). In that approach, the force acting on the particle with polarizability $\hat{\alpha}^{\mathrm{eff}}$ by the field $\tilde{\mathbf{E}}^0$ is $\frac{1}{2}\Re(\mathbf{p}\partial_j\tilde{\mathbf{E}}^{0*})$, which is, however, only one term in the general expression (Equation (2)). Hence, $\hat{\alpha}^{\mathrm{eff}}$ does not always provide a full force description in a system. Moreover, because several terms in Equation (2) depend on $|\alpha|^2$, the gradient forces calculated with a real part of polarizability (as is the case for the free-space Gaussian beam[25]) in a complex environment cannot provide a reliable initial guess.

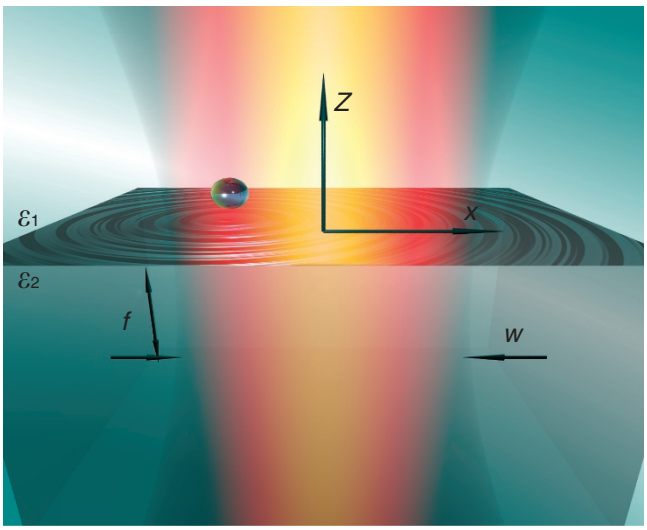

Figure 1 Gaussian beam with waist w is normally incident on a flat silver substrate; the focal position f along the z axis can be either above or below the interface. Optical forces acting on a spherical dielectric particle are formed by beam-particle, beam-substrate and particle–substrate interactions.

Gaussian beam reflected from substrate

To evaluate the background field for the calculation of optical forces, a problem of beam reflection from a surface should be solved. A variety of mathematical models have been adopted for the description of Gaussian beam in free space[24,26–35]. In the context of the optical forces here, tightly focused beams should be described using a non-paraxial model[26–29]. To address the problem of the beam reflection from a dispersive metal instead of a mirror[36], a Fourier decomposition for the Gaussian beam[24,26–28] is more convenient. With this technique, a non-paraxial solution is naturally obtained, whereas other approaches result in cumbersome expressions[29]. The vector description of a Gaussian beam usually implies spatially dependent polarization state[28].

To simplify the analysis and to avoid the aforementioned complications, a two-dimensional (2D) model of p-polarized Gaussian beam is considered here. The focus position f is defined from the origin of the coordinates, and its position along the z axis is kept as a parameter (Figure 1). The beam satisfies Maxwell's equations and has the longitudinal field component. The scalar magnetic field is obtained according to the standard approach[24], and the non-paraxial electric field components of the beam of waist w, taking into account Fresnel reflection coefficients r_p for spatial harmonics, are given by

$$\begin{aligned} \tilde{\mathrm{E}}_x^0 &= \tfrac{w}{2\sqrt{\pi}}\int_{-k_1}^{k_1}\tfrac{k_{z_1}}{k}\mathrm{e}^{-\frac{k_x^2w^2}{4}}\mathrm{e}^{ik_{z_1}f}(\mathrm{e}^{-ik_{z_1}z} - r_p\mathrm{e}^{ik_{z_1}z})\mathrm{e}^{ik_x x}\mathrm{d}k_x \\ \tilde{\mathrm{E}}_z^0 &= \tfrac{w}{2\sqrt{\pi}}\int_{-k_1}^{k_1}\tfrac{k_x}{k}\mathrm{e}^{-\frac{k_x^2w^2}{4}}\mathrm{e}^{ik_{z_1}f}(\mathrm{e}^{-ik_{z_1}z} + r_p\mathrm{e}^{ik_{z_1}z})\mathrm{e}^{ik_x x}\mathrm{d}k_x \end{aligned} \tag{4}$$

doi:10.1038/lsa.2016.258

Each of the harmonics of upper half-space has a transverse component of wave vector k_x and a vertical component $k_{z1} = \left(k_1^2 - k_x^2\right)^{1/2}$. To shift the position of Gaussian beam along the z axis to the focal point f, the phase shift $e^{ik_{z1}f}$ is introduced[24]. The reflected beam has a Gaussian profile with the focal position and propagation direction inverted relative to the incident beam through the reflection from the imaginary plane lying on the interface. Notably, in the integral approach, a proper inclusion of evanescent modes in a free-space Gaussian beam can be applied only to half-spaces[31]. This implies that evanescent fields can be included either in the incident or reflected beams in Equation (4); thus, integration limits are set to $\pm k_1$ to restrict contributing harmonics to the propagating modes only. By inserting $k_{z1} = k_1 - k_x^2/(2k_1)$ to the integrals of Equation (4), the paraxial solution can be obtained (Supplementary Information E). However, the non-paraxial model is employed hereafter to avoid any limitations, and the paraxial model is used only for certain analytical estimations to gain intuitive insights regarding the effects.

RESULTS AND DISCUSSION

Plasmonic trapping and anti-trapping

A semi-infinite metal substrate supports surface plasmon-polariton waves with a high-frequency cutoff corresponding to the resonant surface excitation. In an ideal case, the resonant condition occurs when $\varepsilon_2 = -\varepsilon_1$, whereas for tabulated silver[37] interfacing with air, the plasmon resonance occurs at the wavelength $\lambda = 342$ nm, $\varepsilon_2 = -1.25{+}0.32i$ because of material losses. All the forces calculated hereafter are normalized to the force F_G along z direction exerted on the particle placed at the center of the focal spot of free-space Gaussian beam. In the paraxial approximation, the radiation pressure on the particle positioned at the center of the beam ($x = 0$, $z = 0$) is $F_G = \left(1 - k_1^{-2}w^{-2}\right)\left(k_1^2 + 3k_1^{-2}w^{-4} - 2w^{-2}\right)\mathrm{Im}(\alpha)/(2k_1)$. Optical trapping characteristics in the proximity of the beam waist and the impact of the focus position with respect to the surface are studied next. The Gaussian beam is focused either above or below the substrate, and the force acting on a dielectric bead ($\varepsilon = 3$) of radius $R = 15$ nm is calculated (Figure 2). Three different scenarios are considered: glass ($\varepsilon_2 = 2.25$) and silver substrates, and in the latter case, the plasmonic contribution to the optical forces can be switched 'on' and 'off' by either including evanescent harmonics or not (F_{x0}, a force without plasmonic contribution, is evaluated from Equation (2) with integration limits in Green's function set to k_1). For $f = 100$ μm, the bead lying on the substrate (centered at $z = 15$ nm) experiences attraction to the beam center (trapping) for all the cases (Figure 2a). This behavior is typical for a deeply subwavelength low-index bead that has no resonances and is usually attracted towards the axis of a free-space Gaussian beam[2,25]. The comparison between the force values favors the silver substrate, which provides approximately an order-of-magnitude enhancement compared with that of the glass. Moreover, resonant excitation of the plasmon enhances optical force more than twice compared with F_{x0}. Thus, the auxiliary metal substrate increases the trap stiffness using the same laser intensity, thus allowing Brownian motion to be overcome, as shown in Supplementary Information F.

Alternatively, focusing the beam below the substrate ($f = -100$ μm) leads to completely different behavior (Figure 2b). However, for both the glass and the 'silver with plasmon excluded' cases, optical trapping

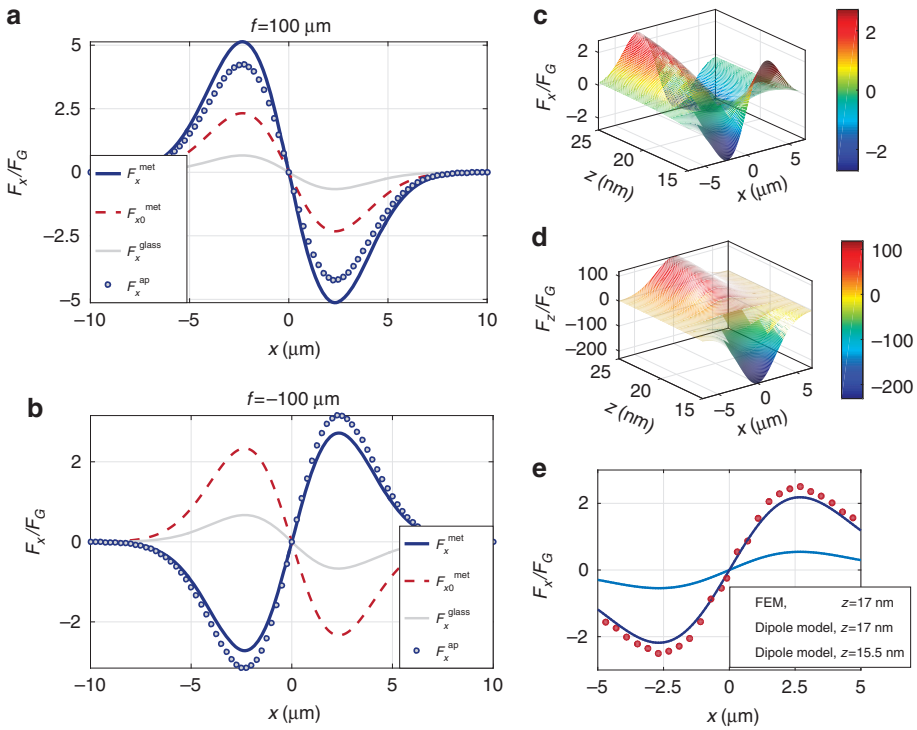

Figure 2 Optical force acting on a particle ($\varepsilon = 3$, radius $R = 15$ nm, $z = 15$ nm) touching the substrate and illuminated by the Gaussian beam focused above ($f = 100$ μm, **a**) or below ($f = -100$ μm, **b**) the substrate interface. Blue solid lines correspond to the silver substrate; red dashed lines correspond to the model without plasmon contribution; gray solid lines correspond to the glass substrate; and dotted lines correspond to the force calculated via approximate Equation (3). (**c**) F_x and (**d**) F_z at $f = -100$ μm as a function of particle position. (**e**) Comparison of the dipole model and the numerical simulation for $f = -130$ μm; the particle is suspended above the substrate. The beam waist diameter $w = 10\lambda$ at the wavelength $\lambda = 342$ nm and the permittivities $\varepsilon_2 = -1.25{+}0.32i$, $\varepsilon_1 = 1$ are used for all plots.

is observed; a real silver substrate leads to optical repulsion from the beam axis, i.e., anti-trapping, pushing the particle away from the region of high optical intensity. The anti-trapping stiffness (derivative of the force with respect to the coordinate) is several times higher than in the case of the glass substrate. A highly confined plasmon mode is a key for achieving this remarkable behavior. Plasmon excitation is correlated with unidirectional rotation of the induced dipole moment of the particle, as shown in Supplementary Information G. This excitation leads to particle motion towards or from the beam axis with beam defocusing relative to the substrate.

The optical forces were investigated as a function of the particle position (Figure 2c and 2d) in order to observe the spatial extent of anti-trapping effect. The plasmonic effect vanishes and standard trapping behavior is observed far from the interface (Figure 2c). In the near-field zone, however, a plasmon-assisted contribution appears to overcome the free-space light-induced potential of the Gaussian beam and governs the interaction, leading to the anti-trapping effect. The vertical force also changes near the interface (Figure 2d). In the far-field zone, an interference pattern is created because of reflection, and as a result, the particle levitates above the surface toward the nearest intensity hot spot. Close to the interface, however, the particle is attracted to the metal and will not levitate because of the near-field interactions. The bead is also repelled from the beam axis.

A finite-element method (FEM) simulation was made in Comsol Multiphysics (Comsol) and Maxwell's stress tensor components were integrated to extract the forces and check the validity of the dipole approximation. First, the geometry in the numerical model was kept the same as in the analytical case study; however, a good match between the analytics and the FEM simulation is achieved if a 1.5 nm offset in the particle position is introduced, i.e., $z=17$ nm versus 15.5 nm in the dipole model, as shown in Figure 2e. This minor fitting is related to the finite size of the particle in the numerical simulations. While both approaches predict an anti-trapping effect, the finite-element simulation suggests slightly higher force values (Supplementary Fig. S4 and Supplementary Information H).

Shifting the focus

In order to reveal the transition between trapping and anti-trapping, the focus position is continuously changed, passing from negative to positive values. The transverse force as a function of both x coordinate and focus position appears in Figure 3a, where anti-trapping is observed for negative f. Plasmon excitation allows noticeable trapping when f is as large as 500 μm. If the plasmon contribution is excluded, then the force appears to be symmetric with respect to f (Figure 3b), and the most efficient trapping occurs at $f=0$. Subtraction of the plasmon-induced contribution to the force (Figure 3c) shows clearly that plasmon excitation is extremely efficient when the beam is focused below the substrate, where the modulus of the ratio $(F_x-F_{x0})/F_G$ reaches values as high as 5, and for positive f, the relative enhancement factor reaches 3 at most. The change in the focal spot position significantly affects the exchange of momentum between the particle, beam and the plasmon, which leads to the asymmetry in the plasmon-assisted optical potential, as shown in Supplementary Information F. Mathematically, asymmetry of $F_x(f)$ is possible according to Equation (2), as it appears in the discussion of the equations. However, F_z (Equation (2)) is symmetric with respect to the sign of f (Supplementary Fig. S1).

Stiffness of the plasmon-assisted optical trap

One of the most important characteristics of optical traps is stiffness. The stiffness defines the localization accuracy and laser intensity required for stable positioning. A nearly linear dependence of the force on the coordinate near the trapping center enables calculation of the force close to the beam axis and assignment of the following value to the stiffness:

$$\gamma_x = -\frac{F_x}{x}|_{x\to 0} \tag{5}$$

By $\gamma_{x0} = -F_{x0}/x$, we denote the force without plasmonic contribution divided by the displacement, and $\gamma_x^{ap} = -F_x^{ap}/x$ is calculated using approximate Equation (3). Hereafter, a particle coordinate will be fixed $x=-0.3$ μm. To assess the stiffness, the transverse force divided by the displacement is plotted in Figure 4 as a function of the focus position f for the two beam waists -10λ and 25λ. The region of anti-trapping (characterized by negative γ_x) begins at a slight offset with respect to $f=0$. The position of the anti-trapping region and its depth depends on the beam parameters: the smaller the beam waist, anti-trapping region is closer to $f=0$. The value of γ_{x0} corresponding to the transverse force without a plasmon behaves similar to light intensity, i.e., symmetric for positive and negative f. By analyzing the plasmon contribution (gray line, Figure 4), one can conclude that plasmon excitation is over twice more efficient at the negative f than at the positive f for the same light intensity.

Both Figures 2 and 4 illustrate that Equation (3) can be taken as a good estimate for the total transverse force at the resonance. Because the Green's function is constant for a particular wavelength and a fixed particle position, a term as simple as $\mathrm{Im}(\tilde{E}_x^0\tilde{E}_z^{0*})$ (defined merely through the excitation field) appears to be responsible for the asymmetric behavior. Starting from the very basics and analyzing the incident beam, we note that the complex field amplitude in free-space Gaussian beam (Supplementary Equation S24), omitting the phase factor that is not relevant in $\mathrm{Im}(\tilde{E}_x^0\tilde{E}_z^{0*})$, changes its sign at the focal plane, as shown in Supplementary Information I. One can

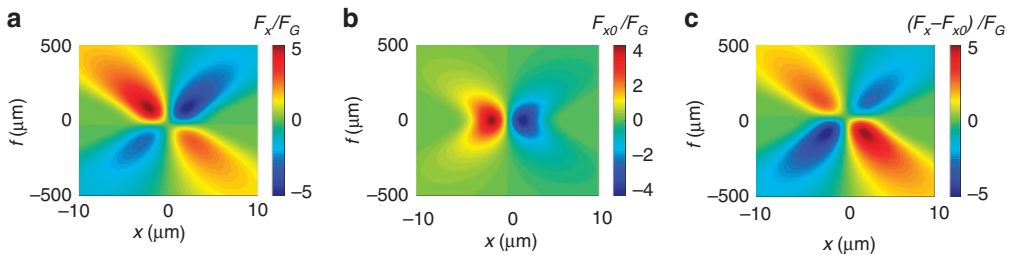

Figure 3 Optical force in a Gaussian beam as a function of particle coordinate (x) across the beam and the beam focus position (f). The particle ($\varepsilon=3$, $R=15$ nm, $z=15$ nm) touches the substrate. (**a**) F_x is the transverse force, (**b**) F_{x0} is the force without plasmonic contribution, (**c**) F_x-F_{x0} plasmon-assisted contribution to the force. The beam parameters are: $w=10\lambda$, $\lambda=342$ nm, dielectric permittivity of the substrate $\varepsilon_2=-1.25+0.32i$ and $\varepsilon_1=1$.

doi:10.1038/lsa.2016.258

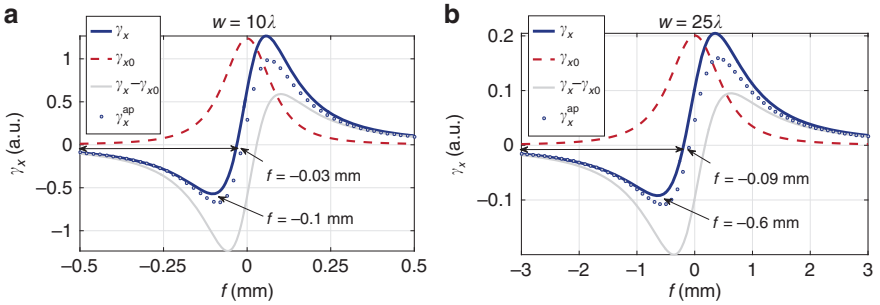

Figure 4 Transverse optical force divided by the displacement of a particle on the substrate ($\varepsilon = 3$, $R = 15$ nm, $x = -0.3$ μm, $z = 15$ nm) for different waists of the Gaussian beam as a function of focal spot position for the silver substrate (solid blue lines); the silver substrate with plasmon contribution excluded (dashed red lines); the plasmon-assisted contribution (solid gray lines); and the estimated according to approximate Equation (3) (dotted lines). Wavelength $\lambda = 342$ nm, $\varepsilon_2 = -1.25 + 0.32i$, $\varepsilon_1 = 1$, beam waist $w = 10\lambda$ (**a**) or $w = 25\lambda$ (**b**).

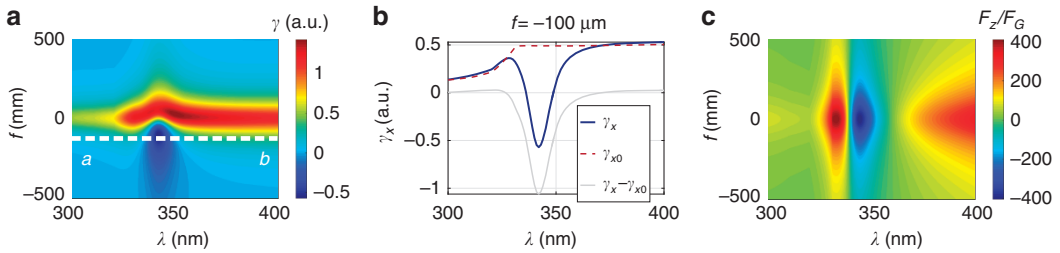

Figure 5 Forces acting on a particle in the Gaussian beam focused on a silver substrate as a function of the focal spot position f and the excitation wavelength λ. Surface plots of (**a**) transverse stiffness γ_x and (**c**) vertical force F_z. (**b**) Transverse force divided by particle displacement at $f = -100$ μm (the *ab* cut in **a**). Particle: $\varepsilon = 3$, $R = 15$ nm, $z = 15$ nm and $x = -0.3$ μm. Beam waist $w = 10\lambda$, $\lambda = 342$ nm, $\varepsilon_2 = -1.25 + 0.32i$ and $\varepsilon_1 = 1$.

immediately envision asymmetry in $\mathrm{Im}(\tilde{E}_x^0 \tilde{E}_z^{0*})$ and F_x with beam shifting.

Optical force and the excitation wavelength

In the previous investigations, the wavelength of the incident beam was chosen to be close to the surface plasmon resonance wavelength. Here, the influence of the wavelength on the trapping characteristics is studied. Figure 5 shows a map of the force spectra for a range of focus positions and excitation wavelengths. In order to assess the trapping and anti-trapping properties, the particle was slightly displaced (by 0.3 μm) from the beam center, and then the lateral force was calculated. The maximal lateral repulsion from the beam occurs near the plasmon resonance. A closer view at the γ_x spectrum for a particular focal position $f = -100$ μm in Figure 5b reveals that the anti-trapping is possible only in the narrow frequency range where plasmon excitation is highly efficient. By focusing the beam at different spots on the z axis, the transverse force F_x and stiffness γ_x change their sign, whereas the vertical force F_z retains direction (Figure 5c). Alternatively, F_z as a function of the excitation wavelength changes its sign at the plasmon resonance. This effect can be explained by the strong phase change on reflection at the resonance and the consequently rapid shift of intensity maxima.

Particle sorting with a plasmonic substrate

One of natural applications of the anti-trapping effect is the sorting of particles. Figure 6 demonstrates the sharp transition from the particle attraction towards the beam axis to particle repulsion away from the beam with the change of beads radii. The effect is possible when the Gaussian beam is focused below the silver substrate at the plasmon resonance. Large particles are trapped, whereas the particles that are small enough are removed from the high field intensity regions at the beam axis. Particles of different radii can be grouped within spatial zones as small as the beam waist of a laser mode. For comparison, other sorting techniques require opposite chiralities of biological objects[20], various shapes of plasmonic particles[38] or different material compositions of nanosamples[25].

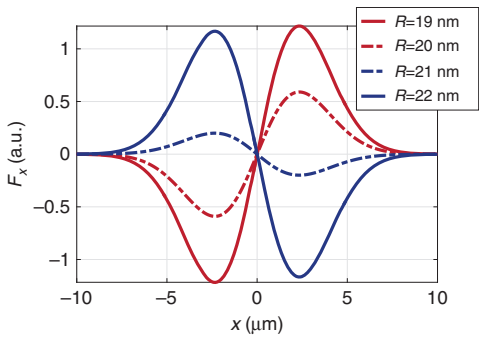

Figure 6 Sorting particles of different radii (specified in the legend) touching the silver substrate. The particle permittivity is $\varepsilon = 3$, Gaussian beam waist is $w = 10\lambda$, and the focus position is $f = -100$ μm, $\lambda = 342$ nm, $\varepsilon_2 = -1.25 + 0.32i$ and $\varepsilon_1 = 1$.

CONCLUSIONS

Plasmonic substrates can essentially affect the performance of optical trapping systems based on focused light beams. It was demonstrated that the shift of the Gaussian beam focus position relative to the

substrate leads to substantial modifications of the optical forces. Either an increase or reduction of the optical trapping stiffness can controllably be achieved. Brownian motion can be overcome using a laser power that is approximately an order-of-magnitude lower than in the case of trapping over a glass substrate. The developed analytical approach emphasizes the contribution of surface waves and suggests that plasmon excitations prevail in opto-mechanical interactions and can even lead to anti-trapping (repulsion from the beam) of a dielectric bead. The ability to switch between the regimes of trapping and anti-trapping opens a venue for efficient sorting of particles and enables dynamic control over the particle location by reconfiguring light by simply moving the beam focus to or from the substrate.

CONFLICT OF INTEREST

The authors declare no conflict of interest.

ACKNOWLEDGEMENTS

This work was supported in part by the Government of the Russian Federation (No 074-U01) and the Russian Fund for Basic Research within the Project No 15-02-01344, 16-52-00112, 16-32-60167, 17-02-01058 and 17-02-01032. The investigation of optical force distributions was supported by the Russian Science Foundation (No 14-12-01227). ASS acknowledges the support of the President of Russian Federation in the frame of Scholarship SP-4248.2016.1, the support of Ministry of Education and Science of the Russian Federation (GOSZADANIE) and BAZIS Fund. AAB acknowledges the RFBR (16-37-60064) and the President of Russian Federation (grant MK-6462.2016.2) for the valuable support. PG acknowledges support from TAU rector grant and German-Israeli foundation (No 2339).

1 Moffitt JR, Chemla YR, Smith SB, Bustamante C. Recent advances in optical tweezers. *Annu Rev Biochem* 2008; **77**: 205–228.
2 Ashkin A, Dziedzic JM, Bjorkholm JE, Chu S. Observation of a single-beam gradient force optical trap for dielectric particles. *Opt Lett* 1986; **11**: 288–290.
3 Roichman Y, Grier DG. Holographic assembly of quasicrystalline photonic heterostructures. *Opt Express* 2005; **13**: 5434–5439.
4 Padgett M, Di Leonardo R. Holographic optical tweezers and their relevance to lab on chip devices. *Lab Chip* 2011; **11**: 1196–1205.
5 Herman RM, Wiggins TA. Hollow beams of simple polarization for trapping and storing atoms. *J Opt Soc Am A* 2002; **19**: 116–121.
6 Porfirev AP, Skidanov RV. Dark-hollow optical beams with a controllable shape for optical trapping in air. *Opt Express* 2015; **23**: 8373–8382.
7 Liu ZR, Zhao DM. Optical trapping rayleigh dielectric spheres with focused anomalous hollow beams. *Appl Opt* 2013; **52**: 1310–1316.
8 Gorkunov MV, Kondratov AV. Macroscopic view of light pressure on a continuous medium. *Phys Rev A* 2013; **88**: 011804.
9 Gramotnev DK, Bozhevolnyi SI. Plasmonics beyond the diffraction limit. *Nat Photonics* 2010; **4**: 83–91.
10 Berkovitch N, Ginzburg P, Orenstein M. Nano-plasmonic antennas in the near infrared regime. *J Phys Condens Matter* 2012; **24**: 073202.
11 Ginzburg P, Arbel D, Orenstein M. Gap plasmon polariton structure for very efficient microscale-to-nanoscale interfacing. *Opt Lett* 2006; **31**: 3288–3290.
12 Righini M, Volpe G, Girard C, Petrov D, Quidant R. Surface plasmon optical tweezers: tunable optical manipulation in the femtonewton range. *Phys Rev Lett* 2008; **100**: 186804.
13 Grigorenko AN, Roberts NW, Dickinson MR, Zhang Y. Nanometric optical tweezers based on nanostructured substrates. *Nat Photonics* 2008; **2**: 365–370.
14 Juan ML, Righini M, Quidant R. Plasmon nano-optical tweezers. *Nat Photonics* 2011; **5**: 349–356.
15 Volpe G, Volpe G, Quidant R. Fractal plasmonics: subdiffraction focusing and broadband spectral response by a Sierpinski nanocarpet. *Opt Express* 2011; **19**: 3612–3618.
16 Righini M, Zelenina AS, Girard C, Quidant R. Parallel and selective trapping in a patterned plasmonic landscape. *Nat Phys* 2007; **3**: 477–480.
17 Shoji T, Tsuboi Y. Plasmonic optical tweezers toward molecular manipulation: tailoring plasmonic nanostructure, light source, and resonant trapping. *J Phys Chem Lett* 2014; **5**: 2957–2967.
18 Volpe G, Quidant R, Badenes G, Petrov D. Surface plasmon radiation forces. *Phys Rev Lett* 2006; **96**: 238101.
19 Min CJ, Shen Z, Shen JF, Zhang YQ, Fang H *et al*. Focused plasmonic trapping of metallic particles. *Nat Commun* 2013; **4**: 2891.
20 Wang SB, Chan CT. Lateral optical force on chiral particles near a surface. *Nat Commun* 2014; **5**: 3307.
21 Rodríguez-Fortuño FJ, Engheta N, Martínez A, Zayats AV. Lateral forces on circularly polarizable particles near a surface. *Nat Commun* 2015; **6**: 8799.
22 Petrov MI, Sukhov SV, Bogdanov AA, Shalin AS, Dogariu A. Surface plasmon polariton assisted optical pulling force. *Laser Photonics Rev* 2016; **10**: 116–122.
23 Shalin AS, Sukhov SV, Bogdanov AA, Belov PA, Ginzburg P. Optical pulling forces in hyperbolic metamaterials. *Phys Rev A* 2015; **91**: 063830.
24 Novotny L, Hecht B. *Principles of Nano-Optics* 2nd edn. Cambridge University Press: New York, NY, USA, 2012.
25 Arias-González JR, Nieto-Vesperinas M. Optical forces on small particles: attractive and repulsive nature and plasmon-resonance conditions. *J Opt Soc Am A* 2003; **20**: 1201–1209.
26 Yariv A. *Quantum Electronics*. 3rd edn. John Wiley & Sons: New York, NY, USA, 1989.
27 Agrawal GP, Pattanayak DN. Gaussian beam propagation beyond the paraxial approximation. *J Opt Soc Am* 1979; **69**: 575–578.
28 Varga P, Török P. The Gaussian wave solution of Maxwell's equations and the validity of scalar wave approximation. *Opt Commun* 1998; **152**: 108–118.
29 Barton JP, Alexander DR, Alexander DR. Fifth-order corrected electromagnetic field components for a fundamental Gaussian beam. *J Appl Phys* 1989; **66**: 2800–2802.
30 Chen CG, Konkola PT, Ferrera J, Heilmann RK, Schattenburg ML. Analyses of vector Gaussian beam propagation and the validity of paraxial and spherical approximations. *J Opt Soc Am A* 2002; **19**: 404–412.
31 Sheppard CJR, Saghafi S. Electromagnetic Gaussian beams beyond the paraxial approximation. *J Opt Soc Am A* 1999; **16**: 1381–1386.
32 Varga P, Török P. Exact and approximate solutions of Maxwell's equations for a confocal cavity. *Opt Lett* 1996; **21**: 1523–1525.
33 Simon R, Sudarshant ECG, Mukunda N. Gaussian-Maxwell beams. *J Opt Soc Am A* 1986; **3**: 536–540.
34 Zauderer E. Complex argument Hermite–Gaussian and Laguerre–Gaussian beams. *J Opt Soc Am A* 1986; **3**: 465–469.
35 Davis LW. Theory of electromagnetic beams. *Phys Rev A* 1979; **19**: 1177–1179.
36 Zemánek P, Jonáš A, Šrámek L, Liška M. Optical trapping of Rayleigh particles using a Gaussian standing wave. *Opt Commun* 1998; **151**: 273–285.
37 Johnson PB, Christy RW. Optical constants of the noble metals. *Phys Rev B* 1972; **6**: 4370–4379.
38 Zharov AA, Shadrivov IV, Zharova NA. Grading plasmonic nanoparticles with light. *Phys Rev A* 2016; **93**: 013814.

Supplementary Information for this article can be found on the *Light: Science & Applications*' website (http://www.nature.com/lsa).